Exp Fluids (2016) 57:81
DOI 10.1007/s00348-016-2171-3

RESEARCH ARTICLE

Delayed lubricant depletion on liquid-infused randomly rough surfaces

Jeong-Hyun Kim[1] · **Jonathan P. Rothstein**[1]

Received: 9 December 2015 / Revised: 19 April 2016 / Accepted: 20 April 2016 / Published online: 4 May 2016

Abstract In this study, pressure drops on liquid-infused superhydrophobic surfaces were measured through a microchannel. A number of different superhydrophobic surfaces were prepared and tested. These surfaces included several PDMS surfaces containing precisely patterned microposts and microridges as well as a number of PTFE surfaces with random surface roughness created by sanding the PTFE with different sandpapers. Silicone oil was selected as the lubricant fluid and infused into the microstructures of the superhydrophobic surfaces. Several aqueous glycerin solutions with different viscosities were used as working fluids so that the viscosity ratio between the lubricant and the working fluid could be varied. The lubricant layer trapped within the precisely patterned superhydrophobic PDMS surfaces was found to be easily depleted over a short period of time even in limit of low flow rates and capillary numbers. On the other hand, the randomly rough superhydrophobic PTFE surfaces tested were found to maintain the layer of lubricant oil even at moderately high capillary numbers resulting in drag reduction that was found to increase with increasing viscosity ratio. The pressure drops on the liquid-infused PTFE surfaces were measured over time to determine the longevity of the lubricant layer. The pressure drops for the randomly rough PTFE surfaces were found to initially diminish with time before reaching a short-time plateau which is equivalent to maximum drag reduction. This minimum pressure drop was maintained for at least three hours in all cases regardless of feature size. However, as the depletion of the oil from the lubricant layer was initiated, the pressure drop was observed to grow slowly before reaching a second long-time asymptote which was equivalent to a Wenzel state.

✉ Jonathan P. Rothstein
rothstein@ecs.umass.edu

[1] Department of Mechanical and Industrial Engineering, University of Massachusetts Amherst, 160 Governors Drive, Amherst, MA 01003-2210, USA

1 Introduction

Superhydrophobic surfaces are rough hydrophobic surfaces containing micron- and/or nanometer-sized surface structures. The combination of the chemical hydrophobicity and the small-scale surface roughness can result in the entrapment of air within the surfaces topography. The presence of this air–water interface has been shown to mobilize liquid droplets on these superhydrophobic surfaces, allowing droplets to slide off easily. This observation is a direct result of the high advancing contact angle, $\theta_A > 150°$, and the low contact angle hysteresis, $\theta_H = \theta_A - \theta_R \approx 5°$, that can be achieved with the right surface design (Kim et al. 2015). The presence of the air–water interface trapped along a superhydrophobic surface can be utilized for laminar or turbulent drag reduction (Daniello et al. 2009; Lauga and Stone 2003; McHale et al. 2009; Ou et al. 2004; Ou and Rothstein 2005; Rothstein 2010; Srinivasan et al. 2013; Truesdell et al. 2006) and to make a surface self-cleaning (Barthlott and Neinhuis 1997; Furstner and Barthlott 2005), anti-fouling (Genzer and Efimenko 2006; Zhang et al. 2005), or anti-icing (Cao et al. 2009; Farhadi et al. 2011). Due to the incredible potential of superhydrophobic surfaces over a broad range of applications and industries, the development of superhydrophobic surfaces has drawn a lot of attention among researchers in the past two decades (Li et al. 2007; Yan et al. 2011).

Unfortunately, there are a number of inherent issues with application of superhydrophobic surfaces that could

hinder their wide-spread adaptation in areas such as drag reduction. The air that is trapped within the structures of the superhydrophobic surfaces can collapse under high static or dynamic pressure (Bocquet and Lauga 2013; Rothstein 2010). Loss of the trapped air can also occur when the superhydrophobic surface is brought in contact with organic liquids or complex mixtures with low surface tension. Additionally, defects introduced during the manufacturing process or mechanical damage incurred during experimentation can also cause a loss of the air–water interface (Bocquet and Lauga 2013; Quere 2008). Without the air–water interface, the attractive benefits of the superhydrophobic surfaces for drag reduction, droplet mobilization, or anti-icing cannot be realized.

Recently, liquid-infused surfaces (LIS) have been developed. These surfaces show great promise to overcome many of the inherent limitations of conventional air-infused superhydrophobic surfaces. Wong et al. (2011), whose work was inspired by the Nepenthes pitcher plant, utilized the small-scale structures of superhydrophobic surfaces as a space to lock in an incompressible and immiscible lubricant. They demonstrated that the liquid-infused surfaces had a number of interesting properties including: liquid repellency of various simple and complex liquids with low surface tension, robustness under high pressure, and restoration of liquid repellency after physical damage. Several research groups have investigated further potential benefits of liquid-infused surfaces (Epstein et al. 2012; Kim et al. 2012; Lafuma and Quere 2011; Smith et al. 2013; Solomon et al. 2014; Subramanyam et al. 2013). Here, we will focus on the application of liquid-infused surfaces to drag reduction.

Using a cone-and-plate rheometer, Solomon et al. (Solomon et al. 2014) measured the drag forces on liquid-infused surfaces. Their surfaces were fabricated from a silicon wafer using a laser ablation process that resulted in a surface with 50-μm-tall posts spaced roughly 50 μm apart with nanometer-scale roughness decorating the sides and tops of the posts. A series of different viscosity oils were used to coat the rough silicon surface, while the working fluid was a water–glycerin mixture. The viscosity ratio, μ_w/μ_o, between the working fluid and the lubricating oil was varied from approximately $\mu_w/\mu_o = 0.03$ to 260. Here, μ_w is the viscosity of the bulk aqueous phase and μ_o is the viscosity of the oil phase infused into the surface. Solomon et al. (2014) demonstrated that an increase in drag reduction could be achieved with increasing viscosity ratio resulting in a maximum drag reduction of 16 % and an equivalent slip length of 18 μm for the case with the largest viscosity ratio tested, $\mu_w/\mu_o = 260$. One advantage to using a cone-and-plate rheometer to measure drag reduction in liquid-infused surfaces is that the imposed flow has closed streamlines. As a result, depletion of oil from lubricating layer with time in the flow direction is negligible and does not affect the measured drag reduction. Jacobi et al. (2015a, b) showed that fluid–fluid interface can be rearranged by the centripetal pressure gradient; however, they showed that the presence of microstructure and the concentric pinning lines that Solomon et al. (2014) etched onto the surface would mitigate radial oil depletion as well. However, for flows without closed streamlines, like the flow through a microchannel studied here, loss of oil from the lubricating layer can be a serious problem (Jacobi et al. 2015a, b; Wexler et al. 2015a, b). This is because to obtain drag reduction, a nonzero slip velocity is produced at the interface between the bulk fluid and the lubricating fluid, whether air or oil (Ou and Rothstein 2005). This slip velocity can be 50 % or more of the average bulk free-stream velocity. As a result, the flow of the bulk fluid imparts a nonzero velocity to the lubricating fluid trapped within the rough surface. For flow within a microchannel, therefore, oil is driven along the liquid-infused surfaces from the inlet to the outlet where it is either swept away or forced to recirculate within the lubricating layer, thereby reducing its effectiveness for drag reduction. As a result, in some cases, continuous injection of the lubricant from a reservoir is necessary for prolonged operation of liquid-infused surfaces (Solomon et al. 2014; Wong et al. 2011).

In this study, systematic measurements of the pressure drop for the flow past a series of liquid-infused surfaces in a microchannel will be presented. To test the impact of surface design on drag reduction, the lubricating oil was infused into a series of superhydrophobic surfaces containing both precisely engineered patterns of microposts and microridges as well as randomly rough superhydrophobic surfaces fabricated by sanding PTFE with various sandpaper grits. The longevity of the lubricant layer on each surface was studied with both microscopy and time-resolved pressure drop measurements. The experimental results demonstrate that, for the surfaces studied here, the randomly rough liquid-infused surfaces were more effective at maintaining the lubricating oil layer. However, it should be noted that, even for the most effective surfaces tested, a loss in performance was observed with time. These measurements presented here will provide potential applicability and limitations of liquid-infused surfaces to microfluidic devices and large-scale drag reduction applications such as turbulent drag reduction in pipelines and along ship hulls.

2 Experiments

In the experiments presented here, the drag reduction in flow past liquid-infused surfaces was measured using a microchannel geometry. A schematic diagram of the microfluidic flow cell used to make pressure drop measurements

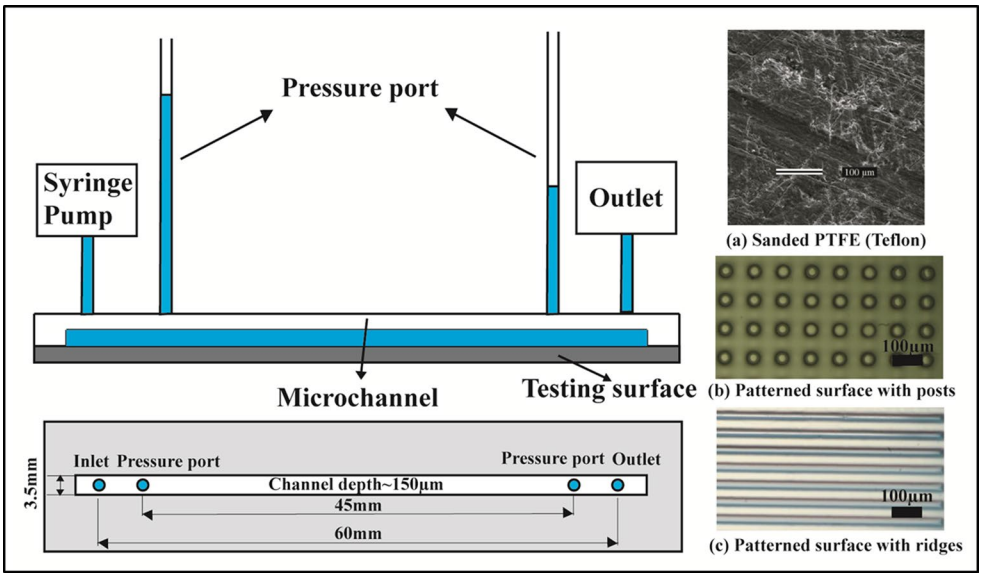

Fig. 1 Schematic diagram of the experimental set up used for pressure drop measurements. Also included are **a** a scanning electron microscopy image of a PTFE surface sanded with 240-grit sandpaper (RMS roughness of 13.7 μm) and optical microscope images of **b** a PDMS surface consisting of 50-μm posts spaced 50 μm apart, and **c** a PDMS surface containing 30-μm ridges spaced 30 μm apart

is shown in Fig. 1. The microfluidic device consists of three parts: a rectangular microchannel, testing surfaces, and two clamps used to seal the microchannel. The microchannel was fabricated from polydimethylsiloxane (PDMS) (Sylgard 184, Dow Corning) using a standard soft lithography method. An inlet and an outlet for the flow of working fluids were introduced at the ends of the microchannel and spaced 60 mm apart. In addition, two pressure ports were created in the microchannel 45 mm apart to measure the pressure drops across the liquid-infused surfaces. The microchannel was attached to an acrylic cover slip to increase its rigidity and distribute the clamping force uniformly across the device. Due to the low modulus (~1.8 MPa) of the PDMS, the microchannel was deformed slightly when it was sealed resulting in an actual microchannel depth measured to be 150 μm through microscopy and fits to the pressure drop measurements from flow past smooth PTFE surfaces. Note that the effect of the side walls of the microchannel is negligible in our experimental set up due to its high aspect ratio (23:1) (Song et al. 2014). As a result, for the purposes of theoretical pressure drop calculations, the channel can be assumed to be equivalent to two infinite parallel plates without introducing significant error.

In order to create a series of randomly rough superhydrophobic surfaces to test as liquid-infused surfaces, smooth polytetrafluoroethylene (PTFE) surfaces (McMaster-Carr) were sanded by several grits of sandpapers (McMaster–Carr) to impart small-scale surface features (Nilsson et al. 2010; Song et al. 2014). A scanning electron microscopy (SEM) image of the resulting PTFE surfaces is shown in Fig. 1a. This technique for fabricating superhydrophobic surfaces was initially developed by Nilsson et al. (Nilsson et al. 2010). They demonstrated that superhydrophobic surfaces with very large advancing contact angles, $\theta_A \approx 150°$, and extremely low contact angle hysteresis, $\theta_H \approx 5°$, could be generated using a 240-grit sandpaper. In addition, they demonstrated that the advancing contact angle and the contact angle hysteresis could be controlled by selection of sandpapers and the surface roughness that it imparts onto the PTFE. To produce the sanded PTFE surfaces, a smooth PTFE surface was first glued to the microscope glass with epoxy to keep the surface flat and smooth. The surface was then sanded by hand with a sanding motion biased in the flow direction using sandpaper grits of 180, 240, and 320 (Song et al. 2014). The resulting RMS surface roughness was measured to be 15.4, 13.7, and 10.9 μm for 180, 240 and 320 grits of sandpaper based on the literature (Nilsson et al. 2010). To maximize consistency between surfaces, the sanding was performed for the same amount of time and applied pressure for each surface. However, given the variation resulting from the fabrication process, it was important to perform experiments using a number of different sanded PTFE surfaces. For each experimental data point presented here, at a minimum, three surfaces were fabricated and tested independently so that experimental uncertainty could be assessed (Song et al. 2014). Following the sanding of the surfaces, a residue of PTFE particles remained and was removed from the surface by first blowing them off with compressed air and then performing a final rinse with distillated water. The surfaces were then allowed to air dry before being coated with the lubricating fluid.

The precisely patterned superhydrophobic surfaces were fabricated in PDMS using standard soft lithography methods (Ou et al. 2004; Whitesides and Stroock 2001). The masks used for the fabrication of master wafers were printed on a high-resolution transparency with a resolution of 20,000 dpi, thus allowing for features as small as

10 μm. The pattern was transferred from the mask to the wafer using mask aligner and a photoresist (SU-8) resulting in a surface topography that was a negative of the desired superhydrophobic surface. For these experiments, the patterns consisted of circular microposts and microridges with a diameter/width 50 and 30 μm, respectively, as shown in Fig. 1b, c. The spacing between the microridges was varied from 30 to 60 μm, while the features were all 25 μm tall. To create the superhydrophobic surface, polydimethylsiloxane (PDMS) (Sylgard 184, Dow Corning) was cast onto the silicon master and cured overnight at 60 °C. After gently peeling the PDMS from the silicon master, it was ready to be coated with the lubricating oil.

In order to produce drag reduction, the lubricant fluid within the liquid-infused surfaces must not be miscible with the working fluids (Solomon et al. 2014; Wong et al. 2011). A number of different oils were tested before selecting silicone oil. Silicone oil was chosen because it was found to fully wet the surface features of both the PDMS and PTFE in the presence of both air and the working fluid. Furthermore, it was crucial to select a lubricant with low viscosity so that the ratio of the viscosity of the working fluid, μ_w, and the viscosity of the lubricating oil, μ_o, could be as large as possible, $\mu_w/\mu_o \gg 1$. To accomplish this, silicone oil with a viscosity of $\mu_o = 5$cP was chosen. In order to create a uniform coating on the superhydrophobic surfaces, the surface was tilted to 75°. A constant volume of 9 μl of silicone oil was then placed at the top of the surface and allowed to wick into the features on the surface under the combined action of surface tension and gravity. Excess oil was allowed to drain from the bottom of the surface, and any large drops were gently scraped away using a flexible doctoring blade. Note that increasing the volume of oil introduced onto the superhydrophobic surface did not have any effect on drag measurements; however, using less than 9 μl of oil resulted in a surface that was not fully infused with oil and larger initial pressure drop measurements.

For the working fluid, a series of glycerin and water solutions of different compositions were created. They varied in viscosity from that of pure water with the viscosity of $\mu_w = 1$cP to the glycerin and water solutions which had viscosities of $\mu_w = 26$cP and 46cP. Given the viscosity of the silicone oil, viscosity ratios of $\mu_w/\mu_o = 0.2$, 5.2, and 9.2 were achieved. Once the microchannel and the testing surface with a lubricant layer were carefully aligned and sealed (Song et al. 2014), a syringe pump (KD Scientific Model 100) was used to pump the working fluid through the microfluidic device at a constant flow rate. The flow rate was systematically varied to probe the effect of flow velocity on drag reduction for each of the surfaces and viscosity ratios tested. However, so that the experiments at different viscosity ratios could be compared to each other, a set of experiments were all performed at a constant in capillary number of $\mathrm{Ca} = \mu_w U/\gamma = 0.001$. The capillary number compares the relative importance of viscous to interfacial stresses in a flow. Here, U is the average velocity in the microchannel and $\gamma = 29$ mN/m is the interfacial tension between the aqueous working fluid and the lubricating oil (Milosevic and Longmire 2002).

3 Results and discussion

The initial experiments were performed using the precisely patterned PDMS superhydrophobic surfaces. To ensure the quality of the superhydrophobic surface, measurements of drag reduction with the surface in the Cassie–Baxter state, with air trapped between the features of the superhydrophobic surface, were performed and compared to previous measurement in the literature. Measurements of the pressure drop reduction and slip length for the air-infused superhydrophobic surfaces containing 30-μm-wide microridges spaced 30 μm apart were measured to be 40 % and 20 μm, respectively, compared with the measurements for the smooth PDMS surface. These measurements are in agreement with our previously published results for this superhydrophobic surface (Ou et al. 2004). The air was then displaced by coating the superhydrophobic microridge surface with silicone oil as described in the previous section to test the effectiveness of liquid-infused surfaces for drag reduction. The expectation was that for a large viscosity ratio between the aqueous phase and the oil approaching the viscosity ratio between water and air, $\mu_{water}/\mu_{air} = 55$, that similar values of drag reduction would be achieved. Unfortunately, no pressure drop reduction was observed for flow past the liquid-infused surfaces containing 30-μm ridges even at the largest viscosity ratio tested, $\mu_w/\mu_o = 9.2$, when compared to the result of the smooth PDMS surface. To test the effect of flow rate, the flow rate was varied between $0.01\ \mathrm{ml/min} < Q < 1\ \mathrm{ml/min}$ which is equivalent to an average velocity within the microchannel of $0.3\mathrm{mm/s} < U < 31.7\ \mathrm{mm/s}$ and equivalently a capillary number between $0.0005 < Ca < 0.05$. No pressure drop reduction was observed in any of the cases for the precisely patterned liquid-infused surfaces tested. Similar observations were made for liquid-infused surfaces with 30-μm-wide microridges spaced 60-μm-wide and 50-μm microposts spaced 50 μm apart.

To understand this null result, the lubricant layers of patterned surfaces were observed optically before and after the pressure drop measurements using an inverted microscope (Nikon TE2000) with a 10× objective. The microscope images are shown in Fig. 2. The images in Fig. 2a clearly demonstrate that, before the flow is initiated, the silicone oil, which is dyed in Fig. 2a to appear dark, fully wicks into grooves between the microridges on the PDMS surface

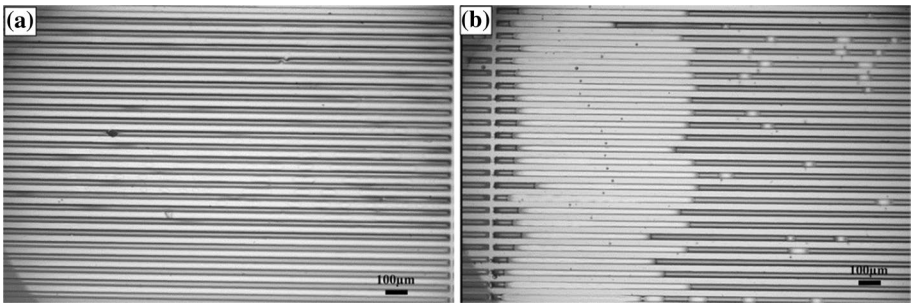

Fig. 2 Microscope images of a superhydrophobic surface patterned with 30-μm spacing microridges **a** before flow showing all the channels between the microridges fully filled with lubricating oil and **b** after a flow of $U = 0.4$ mm/s was applied for $t = 120$ min showing oil partially stripped from between the microridges

creating a uniform lubricating layer. After a flow rate of $U = 0.4$ mm/s with a viscosity ratio between the working fluid and lubricating layer of $\mu_w/\mu_o = 9.2$ was imposed across the liquid-infused surfaces, the image in Fig. 2b clearly shows that the oil within the liquid-infused surface was partially swept away by the flow, driven downstream and removed through the outlet of the microchannel. During the experiment, the working fluid penetrated into and recirculated within the grooves between the microridges, displacing the lubricant and leaving behind grooves that at steady state were only partially filled by lubricant. In some cases, the lubricant that was left behind in the PDMS grooves was observed to contain small droplets of the working fluid. As the flow rate decreases, the rate of depletion of the lubricant layer was slowed. In all cases tested, however, the oil interface was stripped well before the pressure drop measurements reached equilibrium, making it impossible to observe the transient effects on this case. Similar depletion of the lubricant layer was also observed in the case of PDMS liquid-infused surfaces patterned with 50-μm-wide microposts.

A number of additional modifications were made to attempt to stabilize the lubricating oil layer. Silicone oil was initially used, however, with long exposure it was found to cause the patterns on the PDMS surface to swell perhaps facilitating the loss of oil from the liquid-infused surfaces or perhaps causing an increase in the drag masking the expected pressure drop reduction. As an alternative, Miglyol oil, which is commonly used in cosmetics, was chosen as the lubricant fluid. Miglyol oil is known not to swell PDMS (Mulligan and Rothstein 2011) and also can be purchased with a low viscosity, 10cP, and low interfacial tension with pure water, 20 mN/m. On both PDMS superhydrophobic surfaces, however, the depletion of the lubricant layer occurred again even in after lowest capillary number tested, $Ca = 0.0005$.

This failure to maintain fully wicked lubricant layer on patterned liquid-infused surfaces was also observed by Wexler et al. (2015a, b). They used a transparent microfluidic flow cell with a surface patterned with 9-μm-wide grooves spaced 9 μm apart and observed the depletion of silicone oil from the grooves over time. The shear stress from the external flow of water was found to induce a recirculation within the lubricant layer trapped within the micron-sized grooves. The net result was a fast depletion of the lubricant from the downstream end of the surface grooves. At long times, Wexler et al. (2015a, b) showed that a finite length of the lubricant layer remained within the grooves near the outlet port of the microfluidic device. The final wetted length of the grooves was found to depend on interfacial properties of the fluids and the aspect ratio of the patterned surface features. More importantly, the supplements they provide clearly show that microposts of the same height randomly placed on the surface delayed the depletion of the oil from the lubricating layer. It suggests the possibilities to attain the drag reduction on liquid-infused surfaces with random features. To explore this further, here we investigate a surface that is both random in the two-dimensional arrangement of surface topography, but also random in the height of the surface features.

In order to investigate the stability of the lubricant layer on liquid-infused surfaces with three-dimensionally random features, we chose to investigate the effectiveness of a series of sanded PTFE surfaces and measured the pressure drop across these surfaces in the microchannel. Time-resolved pressure drop measurements of the liquid-infused PTFE surfaces are shown in Fig. 3. In this figure, the pressure drops of the PTFE surfaces sanded with 180-grit (RMS roughness of 15.4 μm), 240-grit (RMS roughness of 13.7 μm), and 320-grit (RMS roughness of 10.9 μm) sandpaper are compared for the same viscosity ratio between the aqueous phase and the lubricating oil, $\mu_w/\mu_o = 9.2$, and at a constant average flow velocity of $U = 0.4$ mm/s and a constant capillary number of $Ca = 0.001$. All the surfaces tested exhibited both a short-time (3 h) and a long-time (12 h) plateau in the measured pressure drop. The short-time plateau was reached after approximately 30 min–1 h of flow. Due to the large viscosity of the working fluid and the low flow rates tested, this relatively long start-up time was needed for the working fluid to fully fill the microfluidic device and for the flow to reach equilibrium. Similar start-up times were observed for the case of all sanded PTFE surfaces and were found to be independent of surface roughness. The minimum pressure drops

were maintained for approximately 2 h regardless of the microstructures on the surfaces. As was observed for air-infused superhydrophobic sanded PTFE surfaces (Song et al. 2014), the 240-grit sanded surface was again found to exhibit the lowest pressure drop of the three sanded PTPE surfaces tested. After about 3 h, however, depletion of the lubricant layer was observed through both microscope imaging and oil droplets collecting in the downstream tubing. As a result of the long-time oil depletion, a gradual increase in the measured pressure drop was observed. At large times, unlike the precisely patterned liquid-infused surfaces, the pressure drop settled into a long-time plateau,

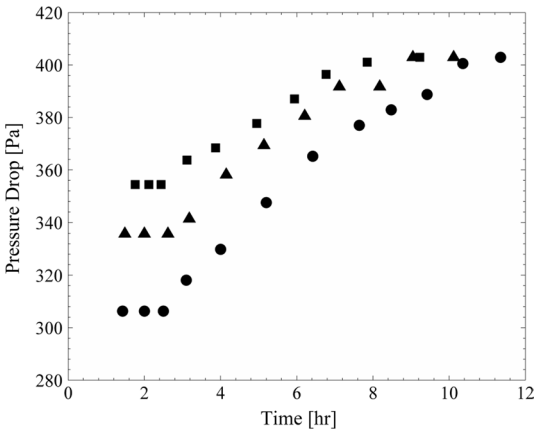

Fig. 3 Pressure drop as a function of time for a series of liquid-infused superhydrophobic sanded PTFE surfaces showing the longevity of the lubricating layer. The experimental data include PTFE surfaces sanded with a series of different sandpaper with grit designation of (*square*) 180 grits, (*circle*) 240 grits, and (*triangle*) 320 grits for the viscosity ratio of $\mu_w/\mu_o = 9.2$. The RMS surface roughness was estimated as 15.4, 13.7, and 10.9 μm for 180, 240, and 320 grits of sandpaper based on the literature (Nilsson et al. 2010). All experiments were performed at a constant flow velocity of $U = 0.4$ mm/s and a constant capillary number of $Ca = 0.001$. The pressure drop data have a maximum uncertainty of 14 Pa

similar to the value observed for these PTFE surfaces in the Wenzel state when the surface roughness was fully wetted by water. These measurements indicate that after 10 h of flow at a capillary number of $Ca = 0.001$ most of the lubricant infused in these sanded PTFE surfaces was depleted from between the surface structures and was replaced by the aqueous working fluid.

To understand the delayed depletion of the lubricant layer on randomly rough surfaces, the surface profile of the PTFE surface sanded with grit designation of 240 grits was measured by Dektak profilometer equipped with stylus of 12.5 μm. Figure 4 shows a 150-μm-wide slice of the profilometer data for sanded PTFE chosen because it was a good representative of the overall surface topography. A sketch of our physical interpretation of the drag reduction data has been superimposed over the surface profile. The standard deviation of the surface roughness was measured to be ±3.1 μm for the range of 150 μm shown in Fig. 4, but, if the surface roughness measured across the entire channel is considered, a standard deviation of ±6.5 μm was measured. During preparation of the liquid-infused surfaces, the lubricant was applied with little shear stress as it was allowed to wick into the surface features and drain slowly down the surface under gravity. As a result, the lubricating oil is likely trapped between the very tallest protrusions of the surface at the start of the drag reduction experiments. We have represented our proposed initial conditions of the liquid-infused surfaces schematically in Fig. 4a. In this hypothetical scenario, the resulting liquid-infused surfaces contain large deep pools of oil and very few solid protrusions. As a result, at the start of each experiment, the interface is nearly shear-free with only a small number of isolated no-slip patches corresponding to the tallest peaks in surface roughness. Under shear flow, these pools will slowly drain, but due to the interconnectivity of the surface, they can be maintained by re-circulation through the three-dimensional surface topography. We believe that

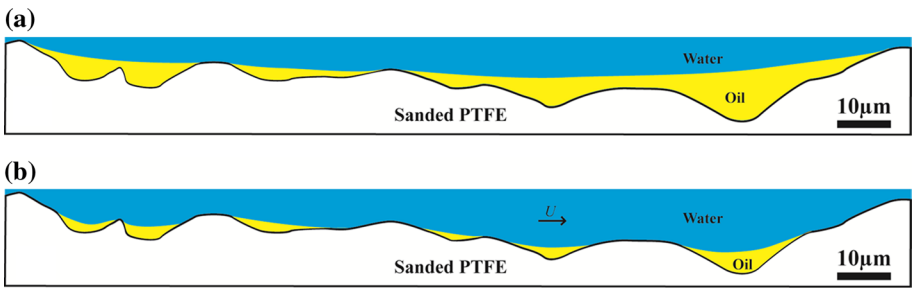

Fig. 4 Lubricant pools on the PTFE surface sanded with grit designation of 240 grits (RMS roughness of 13.7 μm). This 150-μm-long slice of the surface was taken from actual profilometry measurements. It is a representational slice of the sanded PTFE surface. Superimposed on the surface topography is a schematic diagram of the evolution of the oil–water interface which we believe help to explain the experimental results. The initial condition of the surface is shown in (**a**), while in **b** the long-time LIS is shown with oil depleted from the surface

these large nearly shear-free lubricant areas are what lead to the initial minimum in the pressure drop measurements observed for the first 3 h of the experiments as shown in Fig. 3. This emphasizes the importance and value of three-dimensional random surface roughness for establishing and maintaining liquid-infused surface drag reduction. With time, the lubricant layer was depleted, and the depth of the oil layer was slowly reduced. A medium times, $t > 3$ h, the oil layer was stripped sufficiently to begin to reveal additional solid surface features. Finally, at long times, most oil reservoirs have been depleted and only isolated patches of oil on an otherwise rough solid surface remained as we have shown schematically in Fig. 4b. This depletion results in the long time, $t > 12$ h, plateau observed in the data in Fig. 3, which approaches the pressure drop associated with the Wenzel state.

Note that, at short times, the PTFE surface sanded by 240-grit sandpaper had the lowest pressure drop among the sanded surfaces tested while all surfaces approached the same long-time plateau. This trend is consistent with the superhydrophobic drag reduction measurements for sanded PTFE surfaces in the literature (Song et al. 2014). For superhydrophobic drag reduction, Song et al. (2014) argued that the 240-grit sandpaper optimized the feature spacing compared with other sandpaper grits. Increasing the grit size (decreasing the grit designation) increases the width and depth of the scratches and grooves imparted to the PTFE by the sanding process (Nilsson et al. 2010). As the spacing between surface features increases, the slip length and drag reduction are known to increase (Ou et al. 2004; Ybert et al. 2007). However, beyond a critical feature spacing, the air–water interface cannot support a large pressure difference between the water and the air and can collapse to the Wenzel state under flow conditions. For the superhydrophobic sanded PTFE surfaces, this hypothesis is supported by an increase in contact angle hysteresis for sandpaper grit designations smaller than 240. Here, however, the lubricating oil is incompressible and a similar transition is not expected. In fact, the advancing contact angles and contact angle hysteresis for all three liquid-infused surfaces are quite similar at roughly $\theta_A = 100^o$ and $\theta_H = 4^o$ for the 180-grit, 240-grit, and 320-grit sanded PTFE surfaces. The increase in pressure drop from 240 grits to 180 grits is therefore unlikely due to a loss of lubricant from the surface but instead due to the nuances of the initial oil coverage as sketched out in Fig. 4.

Figure 5 shows the time evolution of the pressure drop on the liquid-infused PTFE surface sanded by the 240-grit sandpaper (RMS roughness of 13.7 μm) for three different viscosity ratios. In these measurements, the capillary number was fixed to $Ca = 0.001$ in order to keep the balance between interfacial and viscous stresses consistent between experiments. This was achieved by increasing the flow rate

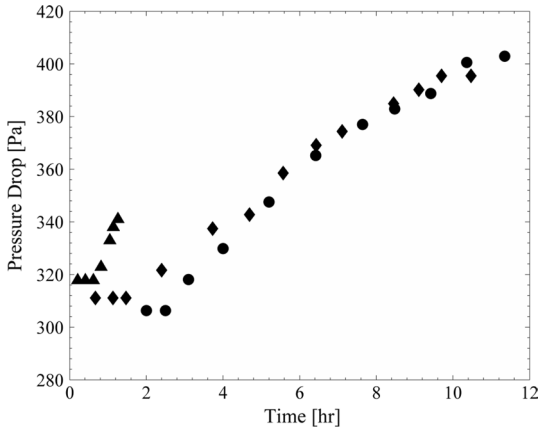

Fig. 5 Pressure drop as a function of time for the liquid-infused superhydrophobic sanded PTFE surfaces sanded with a grit designation of 240 grits (RMS roughness of 13.7 μm) at $Ca = 0.001$. The experimental data include the viscosity ratio of (*triangle*) $\mu_w/\mu_o = 0.2$, (*diamond*) $\mu_w/\mu_o = 5.2$ and (*circle*) $\mu_w/\mu_o = 9.2$. Due to the change in the viscosity of the aqueous phase, to maintain a constant capillary number, the flow velocity increases with decreasing viscosity of the aqueous phase. The pressure drop data have a maximum uncertainty of 14 Pa

as the viscosity of the working fluid was reduced to achieve a smaller viscosity ratio. As the viscosity ratio was reduced from $\mu_w/\mu_o = 9.2$ to 0.2, the short-time minimum in the observed pressure drop was achieved more quickly. This is a direct result of the increased flow rate needed to maintain a constant capillary number of $Ca = 0.001$. For the case of a viscosity ratio of $\mu_w/\mu_o = 0.2$, the short-time minimum pressure drop was maintained for just 1 h. In order to maintain a constant capillary number, the average velocity in the microchannel for the $\mu_w/\mu_o = 0.2$ case was nearly 50 times larger than the $\mu_w/\mu_o = 9.2$ case yet the oil was stripped in only 1/3 the time.

In order to understand the difference in depletion rate of the oil layer quantitatively, we consider the laminar pressure-driven flow between two parallel plates. The top plate is no-slip smooth surface. The bottom plate is slippery rough surface containing oil layer with thickness of t and viscosity of μ_o. This oil layer separates the working fluid with viscosity of μ_w from the bottom plate, generating the height of the water phase, h-t. Here, h is the channel height. By matching shear stress at the oil–water interface, $\mu_w(\partial u_w/\partial y) = \mu_o(\partial u_o/\partial y)$, and assuming Poiseuille flow in the channel, the velocity at the interface is predicted to be $u_o = \left(\mathrm{Ca}\frac{\sigma}{\mu_o}\frac{t}{(h-t)}\right)\left(1 + \frac{\mu_w}{\mu_o}\frac{t}{(h-t)}\right)^{-1}$. In our experiment, the microchannel height was measured to be 150 μm and the oil layer could be assumed to be same order of grit size of the sandpaper, 30 μm. From this calculation, the interfacial velocity for the $\mu_w/\mu_o = 0.2$ case predicted to be three times larger than that of $\mu_w/\mu_o = 9.2$ case. This result is

consistent with our experimental observation shown in Fig. 5, which indicates that the $\mu_w/\mu_o = 0.2$ case begins to lose oil after roughly 1 h while the $\mu_w/\mu_o = 9.2$ case lasts for almost 3 h. Thus, it is clear that capillary number alone does not fully describe the dynamics of lubricating oil depletion. The viscosity ratio also plays an important role as it sets the magnitude of the resulting oil–water interfacial velocity which dictates the mass flux of lubricating oil within liquid-infused surfaces.

Note that the long-time plateau was not observed for the case of a viscosity ratio of $\mu_w/\mu_o = 0.2$ due to the limited capacity of the syringes used in the syringe pump and the fact that even as the flow rate was 50 times larger than the $\mu_w/\mu_o = 9.2$ case, the oil was removed only three times as fast. As a result, a nearly 20-fold increase in syringe volume would have been required to reach steady state for the $\mu_w/\mu_o = 0.2$ case.

From the longevity studies of the lubricant layer in Fig. 5, the effect of viscosity ratio on liquid-infused surfaces drag reduction can be quantified by comparing the average values of the short-time plateau in the pressure drop data to a smooth PTFE surface. A minimum of three measurements with the microfluidic device was recorded. Between each experiment, the device was broken down and reassembled to ensure the repeatability and the robustness of the measurement. In addition to the average pressure drop reduction, the slip length, $b = HD_R/(3 - 4D_R)$, was calculated based on the pressure drop reduction, D_R, and the channel height, H (Ou et al. 2004).

From the data in Fig. 5, a clear increase in the pressure drop reduction and slip length can be observed with increasing viscosity ratio for the 240-grit sanded PTFE surface. The data show linear dependence on viscosity ratio. The mean pressure drop reduction and the slip length on the liquid-infused surfaces were measured to be 10 ± 12, 12 ± 11, and 13 ± 11 % and 6 ± 7, 7 ± 7, and 8 ± 7 μm for the viscosity ratio of 0.2, 5.2, and 9.2, respectively. This linear relationship is expected as it is predicted by the theory developed by Ybert et al. (2007), and shown experimentally by Solomon et al. (2014) for flow within a cone-and-plate rheometer. The error bars on the data represent both the uncertainty of the individual measurements, but also the uncertainty of the channel height which is needed to determine the smooth pressure drop. As discussed earlier, the variation in the surface roughness of the sanded PTFE surface was quite large resulting in a ±6 μm uncertainty in the microchannel height. Within those error bars, the trends in drag reduction and slip length are significant, but these measurements show the challenges in making drag reduction/slip length measurements when the slip length is close to uncertainty in the channel dimensions.

4 Conclusions

The pressure drop measurements on the liquid-infused superhydrophobic surfaces were performed through a microchannel by varying the surface topography and the viscosity ratio between the water and lubricant phases. A low-viscosity, immiscible, and incompressible silicone oil was filled to the gaps between structures of superhydrophobic surfaces. The patterned surfaces with microposts and microridges and randomly rough PTFE surfaces sanded by different grits of sandpapers were prepared for testing surfaces. Several aqueous glycerin solutions with different viscosities were used to change the viscosity ratio. The precisely patterned superhydrophobic surface containing constant height posts and ridges was found ineffective at maintaining a lubricant layer within the microstructure for any measurable length of time even in low capillary numbers, $Ca \approx 0.001$. The shear stress exerted from external flow resulted in a nonzero velocity at the oil–water interface, resulting in a fast depletion of the lubricant from between the microfeatures of liquid-infused surfaces. Conversely, the randomly rough PTFE surfaces, the lubricating oil layer was found to be much longer lived. As a result, a minimum pressure drop corresponding to significant drag reduction was easily maintained for a viscosity ratio of $\mu_w/\mu_o = 9.2$ flowing at $Ca = 0.001$ for more than 3 h. This result was found to be independent to the size of the microstructures introduced into the PTFE by different grit sandpapers. We believe that this is because the three-dimensional patterned surface provided the added pathways for re-circulation of the lubricant. Due to the presence of a small number of high spots (tall posts) on the sanded PTFE surface, it was possible for oil to reside within large pools with nearly complete coverage of the surface topography. Over time the slow depletion of the lubricant layer was found to accelerate most likely as these large oil reservoirs were depleted and its level fall below the top of the tallest surface features. The result was a slow increase in the pressure drop over 10 h before second plateau of the pressure drop was reached. This final pressure drop was equivalent to a Wenzel state. The effect of the viscosity ratio on liquid-infused surfaces was also studied. For a constant capillary number experiment, the lower viscosity ratio liquid-infused surfaces were found to deplete oil and lose their effectiveness more quickly. However, if the experiment were run at constant flow rate, the longevity would increase with reduced viscosity ratio. Our experiments show that the velocity at the oil–water interface is the key to understand lubricant depletion. Finally, the pressure drop reduction and the corresponding slip length were found to increase with increasing viscosity ratio.

Acknowledgments This research was supported by the National Science Foundation under Grant CBET-1334962.

References

Barthlott W, Neinhuis C (1997) Purity of the sacred lotus, or escape from contamination in biological surfaces. Planta 202:1–8

Bocquet L, Lauga E (2013) A smooth future? Nat Mater 10:334–337

Cao L, Jones AK, Sikka VK, Wu J, Gao D (2009) Anti-icing superhydrophobic coatings. Langmuir 25:12444–12448

Daniello R, Waterhouse NE, Rothstein JP (2009) Turbulent drag reduction using superhydrophobic surfaces. Phys Fluids 21:085103

Epstein AK, Wong T-S, Belisle RA, Boggs EM, Aizenberg J (2012) Liquid-infused structured surfaces with exceptional anti-biofouling performance. Proc Natl Acad Sci 109:13182–13187

Farhadi S, Farzaneh M, Kulinich SA (2011) Anti-icing performance of superhydrophobic surfaces. Appl Surf Sci 257:6264–6269

Furstner R, Barthlott W (2005) Wetting and self-cleaning properties of artificial superhydrophobic surfaces. Langmuir 21:956–961

Genzer J, Efimenko K (2006) Recent developments in superhydrophobic surfaces and their relevance to marine fouling: a review. Biofouling J Bioadhesion Biofilm Res 22:339–360

Jacobi I, Wexler JS, Samaha MA et al (2015a) Stratified thin-film flow in a rheometer. Phys Fluids 27:052102

Jacobi I, Wexler JS, Stone HA (2015b) Overflow cascades in liquid-infused substrates. Phys Fluids 27:082101

Kim P, Wong T-S, Alvarenga J, Kreder MJ, Adorno-Martinez WE, Aizenberg J (2012) Liquid-infused nanostructured surfaces with extreme anti-ice and anti-frost performance. ACS Nano 6:6569–6577

Kim J-H, Kavehpour HP, Rothstein JP (2015) Dynamic contact angle measurements on superhydrophobic surfaces. Phys Fluids 27:032107

Lafuma A, Quere D (2011) Slippery pre-suffused surfaces. Europhys Lett 96:56001

Lauga E, Stone HA (2003) Effective slip in pressure-driven stokes flow. J Fluid Mech 489:55–77

Li X-M, Reinhoudt D, Crego-Calama M (2007) What do we need for a superhydrophobic surface? A review on the recent progress in the preparation of superhydrophobic surfaces. Chem Soc Rev 36:1350–1368

McHale G, Shirtcliffe NJ, Evans CR, Newton MI (2009) Terminal velocity and drag reduction measurements on superhydrophobic spheres. App Phys Lett 94:064104

Milosevic IN, Longmire EK (2002) Pinch-off modes and satellite formation in liquid/liquid jet systems. Int J Multiph Flow 28:1853–1869

Mulligan MK, Rothstein JP (2011) The effect of confinement-induced shear on drop deformation and breakup in microfluidic extensional flows. Phys Fluids 23:022004

Nilsson M, Daniello R, Rothstein JP (2010) A novel and inexpensive technique for creating superhydrophobic surfaces using Teflon and sandpaper. J Phys D Appl Phys 43:045301

Ou J, Rothstein JP (2005) Direct velocity measurements of the flow past drag-reducing ultrahydrophobic surfaces. Phys Fluids 17:103606

Ou J, Perot JB, Rothstein JP (2004) Laminar drag reduction in microchannels using ultrahydrophobic surfaces. Phys Fluids 16:4635–4660

Quere D (2008) Wetting and roughness. Annu Rev Mater Res 38:71–99

Rothstein JP (2010) Slip on superhydrophobic surfaces. Annu Rev Fluid Mech 42:89–109

Smith JD, Dhiman R, Anand S et al (2013) Droplet mobility on lubricant-impregnated surfaces. Soft Matter 9:1772–1780

Solomon BR, Khalil KS, Varanasi KK (2014) Drag reduction using lubricant-impregnated surfaces in viscous laminar flow. Langmuir 30:10970–10976

Song D, Daniello R, Rothstein JP (2014) Drag reduction using superhydrophobic sanded Teflon surfaces. Exp Fluids 55:1783

Srinivasan S, Choi W, Park K-C, Chhatre SS, Cohen RE, McKinley GH (2013) Drag reduction for viscous laminar flow on spray-coated non-wetting surfaces. Soft Matter 9:5691–5702

Subramanyam SB, Rykaczewski K, Varanasi KK (2013) Ice adhesion on lubricant-impregnated textured surfaces. Langmuir 29:13414–13418

Truesdell R, Mammoli A, Vorobieff P, van Swol P, Brinker CJ (2006) Drag reduction on a patterned superhydrophobic surface. Phys Rev Lett 97:044504

Wexler JS, Grosskopf A, Chow M, Fan Y, Jacobi I, Stone HA (2015a) Robust liquid-infused surfaces through patterned wettability. Soft Matter 11:5023–5029

Wexler JS, Jacobi I, Stone HA (2015b) Shear-driven failure of liquid-infused surfaces. Phys Rev Lett 114:168301

Whitesides G, Stroock AD (2001) Flexible methods for microfluidics. Phys Today 54:42–48

Wong T-S, Kang SH, Tang SKY et al (2011) Bioinspired self-repairing slippery surfaces with pressure-stable omniphoicity. Nature 477:443–447

Yan YY, Gao N, Barthlott W (2011) Mimicking natural superhydrophobic surfaces and grasping the wetting process: a review on recent progress in preparing superhydrophobic surfaces. Adv Colloid Interface Sci 169:80–105

Ybert C, Barentin C, Cottin-Bizonne C, Joseph P, Bocquet L (2007) Achieving large slip with superhydrophobic surfaces: scaling laws for generic geometries. Phys Fluids 19:123601

Zhang H, Lamb R, Lewis J (2005) Engineering nanoscale roughness on hydrophobic surface-preliminary assessment of fouling behavior. Sci Technol Adv Mater 6:236–239